Characterization of an electron conduit between bacteria and the extracellular environment

Robert S. Hartshorne[a], Catherine L. Reardon[b], Daniel Ross[c], Jochen Nuester[d], Thomas A. Clarke[a], Andrew J. Gates[a], Paul C. Mills[a], Jim K. Fredrickson[b], John M. Zachara[b], Liang Shi[b], Alex S. Beliaev[b], Matthew J. Marshall[b], Ming Tien[c], Susan Brantley[d], Julea N. Butt[a], and David J. Richardson[a,1]

[a]School of Biological Sciences, University of East Anglia, Norwich NR4 7TJ, United Kingdom; [b]Pacific Northwest National Laboratory, P.O. Box 999, Richland, WA 99352; and Departments of [c]Biochemistry and Molecular Biology, and [d]Geoscience, Pennsylvania State University, University Park, PA 16802-4500

Edited by Dianne Newman, Massachusetts Institute of Technology, Cambridge, MA, and accepted by the Editorial Board September 9, 2009 (received for review January 7, 2009)

A number of species of Gram-negative bacteria can use insoluble minerals of Fe(III) and Mn(IV) as extracellular respiratory electron acceptors. In some species of *Shewanella*, *deca*-heme electron transfer proteins lie at the extracellular face of the outer membrane (OM), where they can interact with insoluble substrates. To reduce extracellular substrates, these redox proteins must be charged by the inner membrane/periplasmic electron transfer system. Here, we present a spectro-potentiometric characterization of a trans-OM *icosa*-heme complex, MtrCAB, and demonstrate its capacity to move electrons across a lipid bilayer after incorporation into proteoliposomes. We also show that a stable MtrAB subcomplex can assemble in the absence of MtrC; an MtrBC subcomplex is not assembled in the absence of MtrA; and MtrA is only associated to the membrane in cells when MtrB is present. We propose a model for the modular organization of the MtrCAB complex in which MtrC is an extracellular element that mediates electron transfer to extracellular substrates and MtrB is a trans-OM spanning β-barrel protein that serves as a sheath, within which MtrA and MtrC exchange electrons. We have identified the MtrAB module in a range of bacterial phyla, suggesting that it is widely used in electron exchange with the extracellular environment.

cytochrome-*c* | iron respiration | protein film voltammetry | electron paramagnetic resonance | *Shewanella*

A number of species of Gram-negative bacteria can couple anaerobic growth to the respiratory reduction of mineral-oxides, such as those of Fe(III) and Mn(IV), that are insoluble in water at neutral pH and so unable to enter the cell (1). Energy conservation in Gram-negative bacteria relies on the generation of a proton-motive force across the inner membrane (IM). Electrons reduce the IM quinone (Q) pool to quinol (QH_2) via the activity of proton-motive enzymes, such as formate dehydrogenase or hydrogenase (1). In order for continued turnover, the QH_2 pool needs to be reoxidized. For water soluble electron acceptors, the systems that perform this function are associated with the IM or periplasm, where access to the active sites of these enzymes is straightforward. However, cycling the QH_2 pool is a problem when the available electron acceptor cannot enter the cell, as in the case of Fe(III) minerals. One of the electron-transfer models proposed for extracellular Fe(III) reduction in *Shewanella* species implicates *deca*-heme *c*-type cytochromes encoded by the *omcA-mtrCAB* gene cluster (2–5). MtrC and OmcA are located on the extracellular face of the outer membrane (OM), where they can be directly involved in electron transfer to extracellular Fe(III) minerals (6, 7), or to extracellular electron shuttles, which in turn reduce Fe(III) minerals not physically associated with the cell (8, 9). Importantly, electron delivery to the extracellular *deca*-heme cytochromes requires that electrons originating from the IM are transferred across the OM. The biochemical basis for this electron transfer is not understood. MtrB is predicted to be an OM β-barrel porin comprising 28 transmembrane β-strands that is critical for extracellular Fe(III) respiration (10). However, the role performed by MtrB in electron transfer across the OM is unclear, because its amino acid sequence does not display a canonical redox cofactor binding motif (Fig. S1). MtrA is predicted to be a *deca*-heme periplasmic protein (Fig. S1) (10), which associates with the OM as part of an MtrCAB complex (5). Because the OM is ≈40 Å wide, and MtrA and MtrC are predicted to be on opposite sides of it, it is not immediately obvious how electrons can pass between them in vivo. This study presents a characterization of the MtrCAB complex that leads us the propose a novel trans-OM electron transfer system, in which the MtrB porin serves as a sheath within which MtrA and MtrC can embed sufficiently at the inner and outer faces of the membrane, respectively, for electron transfer to take place between them.

Results and Discussion

Spectral Characterization of the MtrCAB Complex in Micelles and Liposome Membranes. The MtrCAB complex was purified from cell membranes of *Shewanella oneidensis* solubilized in Triton X-100 (TX100) (Fig. S2). SDS/PAGE revealed that two subunits stained for heme-dependent peroxidase activity (Fig. 1*A*), which were confirmed as MtrC (≈85 kDa) and MtrA (≈40 kDa) by probing with specific antibodies. An additional band running slightly slower than MtrC was also visualized on gels stained with Coomassie blue (Fig. 1*B*). Cross-reactivity toward MtrB antibody and analysis by MS confirmed that this protein was the OM β-barrel porin MtrB. Analysis of the MtrCAB preparations by sedimentation equilibrium (SE) at a range of concentrations (0.25–2.5 μM) and rotation rates (7, 9, and 11 krpm) confirmed that the protein behaved as a single homogenous species with an apparent molecular mass (M_w^{app}) of ≈210 kDa (Fig. 2*A*), consistent with a 1:1:1 ratio of MtrCAB in a heterotrimeric *icosa*-heme complex (6). The solution UV-visible spectrum of MtrCAB in TX100 micelles is typical of low spin *c*-type cytochromes with absorption maxima at 410 nm (γ) and 540 nm in the oxidized state and 422 nm (γ), 520 nm (β), and 552 nm (α) in the reduced state (Fig. 3*A*). To assess whether MtrCAB can catalyze transmembrane electron transfer, the complex was incorporated into liposomes with the redox dye methylviologen (MV) entrapped within the vesicles. In control experiments, it was established that addition of dithionite (up to 170 μM) to the MV-liposomes in the absence of the MtrCAB complex did not result in the reduction of the internalized MV (Fig. S3*A*). However, when the MV-liposomes were solublized using TX100 reduction of the MV did occur as indicated by the development of the reduced peaks at ≈395 and ≈600 nm (Fig. S3*A*). When MV-proteolipo-

Author contributions: R.S.H., C.L.R., T.A.C., J.K.F., J.M.Z., L.S., A.S.B., M.J.M., M.T., S.B., J.N.B., and D.J.R. designed research; R.S.H., C.L.R., D.R., J.N., T.A.C., A.J.G., P.C.M., L.S., A.S.B., and M.J.M. performed research; R.S.H., C.L.R., D.R., J.N., T.A.C., A.J.G., and J.N.B. analyzed data; and T.A.C., J.K.F., J.M.Z., M.T., S.B., J.N.B., and D.J.R. wrote the paper.

The authors declare no conflict of interest.

This article is a PNAS Direct Submission. D.N. is a guest editor invited by the Editorial Board.

[1]To whom correspondence should be addressed. E-mail: d.richardson@uea.ac.uk.

This article contains supporting information online at www.pnas.org/cgi/content/full/0900086106/DCSupplemental.

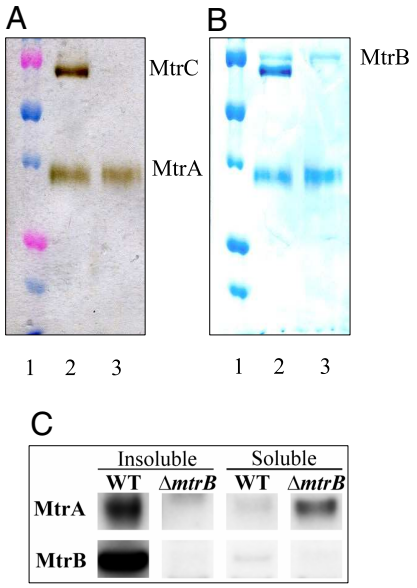

Fig. 1. SDS/PAGE analysis of Mtr proteins. (*A* and *B*) Two replica samples were resolved by 12% (wt/vol) SDS/PAGE and stained for heme-dependent peroxidase activity (*A*) or with Coomassie blue (*B*). Lane 1, molecular mass markers (from top of gel: 100, 75, 50, 37.5, 25, and 15 kDa); lane 2, MtrCAB; lane 3, MtrAB. (*C*) Soluble and insoluble fractions of *S. oneidensis* WT and Δ*mtrB* strains probed using MtrA- and MtrB-specific antibodies.

somes were prepared with MtrCAB incorporated, the spectral feature of oxidized MtrCAB was apparent through the γ-band feature at 410 nm (see black spectrum in Fig. 3*B*). Control experiments in which the liposomes were sedimented by ultracentrifugation confirmed that the cytochrome was associated with the membrane vesicles and not the supernatant. Addition of dithionite to the MtrCAB MV-proteoliposomes resulted in reduction of the MtrCAB hemes as indicated by a shift of the γ-band from 410 to 422 nm and the development of the α-peak at 552 nm (see red spectrum in Fig. 3*B*). Reduction occurred within 1 min of adding the dithionite (Fig. S3*B*). The extent of reduction of the cytochrome did not increase significantly when the MV-proteoliposomes were solublized in TX100 (see blue spectrum in Fig. 3*B*; note that the background light-scattering was decreased as a consequence of the dissolution of the liposomes in the detergent in Fig. S3*B*). The features of the reduced minus oxidized difference spectra (see red line in Fig. 3*B Inset*) were similar to those of the MtrCAB protein in solution (see black line in Fig. 3*B Inset*), confirming that there was significant reduction of the MtrCAB hemes and demonstrating that electrons from dithionite could equilibrate across all of the MtrC and MtrA hemes in the proteoliposomes. Significantly, the spectral features of reduced MV also developed when dithionite was added to the MtrCAB MV-proteoliposomes (see red spectrum in Fig. 3*B*). These features are partially obscured by the reduced MtrCAB absorption spectrum and the light scattering from the liposomes; however, the sharp 395-nm absorption band and broad ≈600-nm absorption bands characteristic of reduced MV could be clearly resolved in the reduced *minus* oxidized difference spectra of the proteoliposomes (see red line in Fig. 3*B Inset*), and were absent from the reduced *minus* oxidized difference spectrum of the MtrCAB in solution (see black line in Fig. 3*B Inset*). Control experiments were carried out in which proteoliposomes were ultracentrifuged after treatment with dithionite. The supernatants were collected and reduced with dithionite. No signals characteristic of reduced MV were apparent (Fig. S3*D*), which confirmed that the proteoliposomes did not leak MV after this treatment.

The liposome experiments demonstrate that at least some of the MtrCAB molecules reconstitute into MV-proteoliposomes in a topology that allows them to mediate electron transfer between externally added dithionite and the entrapped MV, the functionality of the complex in transmembrane electron transfer. Addition of Fe(III) citrate to the dithionite-reduced MV-proteoliposomes resulted in reoxidation of the MtrCAB complex as judged by the shift of the γ-band from 422 to 410 nm and disappearance of the 552 nm peak (see green spectrum in Fig. 3*B*). Reoxidation of the internalized reduced MV also occurred as indicated by the disappearance of the 395 and 600 nm absorption bands of reduced MV, which can be seen against the light-scattering background of the proteoliposomes (see green spectrum in Fig. 3*B*) and in redox difference spectra (Fig. S3*C*). This result demonstrates that a proportion of the MtrCAB molecules in the MV-proteoliposomes are able to mediate electron transfer between internalized reduced MV and external Fe(III) citrate. Spectra collected on dithionite-reduced supernatants collected after centrifugation of the samples showed no signals characteristic of reduced MV, confirming that Fe(III) citrate treatment did not make the MV-proteoliposomes leaky. The question of whether there are two different orientations of MtrCAB that work in mediating electron transfer in different directions [dithionite → MV and reduced MV → Fe(III) citrate] or whether MtrCAB can transfer electrons bidirectionally cannot be answered at this stage, but together, the experiments in this section directly show the ability of the MtrCAB complex to move electrons across a lipid bilayer.

Thermodynamic Properties of the MtrCAB Complex. Visible spectra of the MtrCAB complex were collected from samples equilibrated at various potentials. The α-peak intensity decreased on lowering the potential, but its shape and position were indistinguishable from those displayed by the fully reduced protein (Fig. 3*A Inset*). The absorbance at 552 nm plotted as a function of equilibration potential showed that the hemes within MtrCAB were reversibly reduced and oxidized over a potential range spanning ≈450 mV, from fully

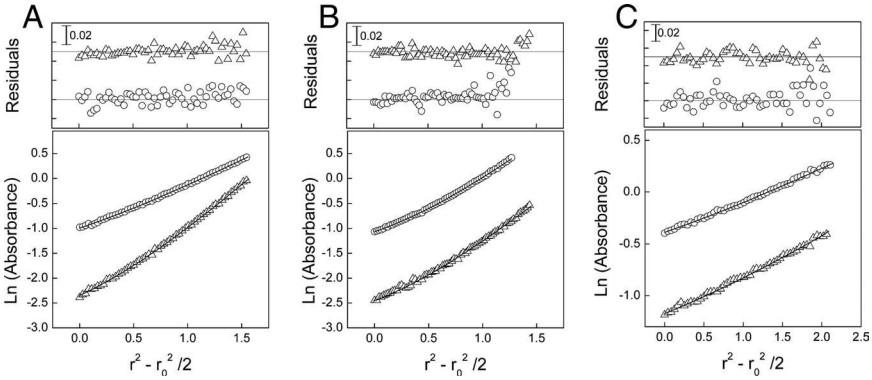

Fig. 2. SE analysis of the Mtr proteins. (*A*) Absorbance profiles of 0.7 μM MtrABC (triangles) and 2.5 μM MtrAB (circles) measured at 435 nm and 9 krpm. (*B*) Absorbance profiles of MtrAB and MtrC at 0.4 μM (triangles) and 0.1 μM (circles) measured at 435 and 410 nm, respectively, at 8 krpm. (*C*) Absorbance profiles of 10 μM MtrC (triangles) and MtrA (circles) measured at 530 nm and 8 krpm. The lines represent fits to a single species. At top are shown residual differences between the experimental data and fitted curves.

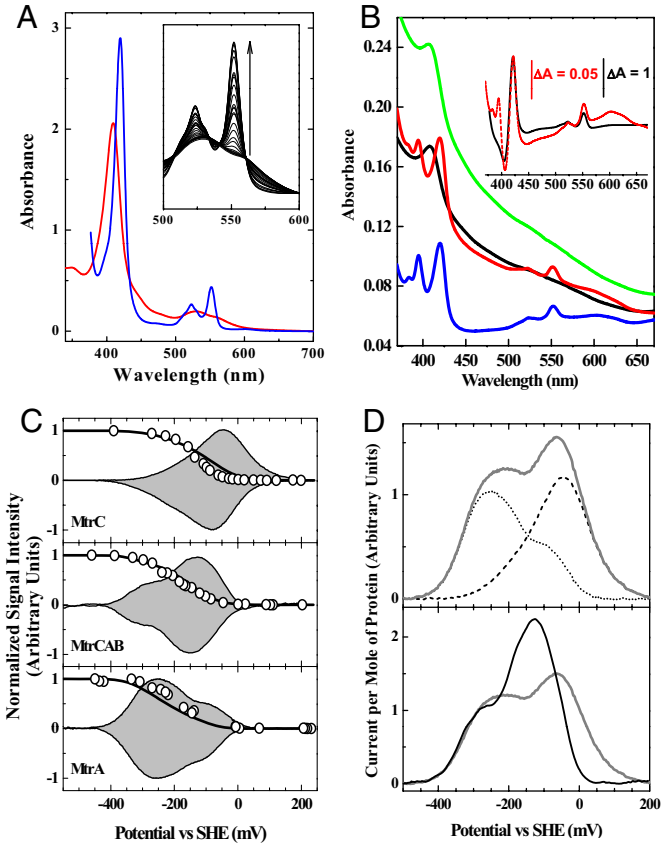

Fig. 3. Spectropotentiometric properties of the Mtr proteins. (*A*) Oxidized (red spectrum) and reduced (blue spectrum) UV-vis spectra of 2 μM MtrCAB. (*Inset*) Successive UV-vis spectra of MtrCAB recorded during reductive titration (arrow indicates increasingly negative solution). (*B*) UV-vis spectra of MtrCAB MV-proteoliposomes. Black, oxidized; red, reduced for 1 min with 5 μM dithionite; blue, 1 min after addition of 1% TX100 to the dithionite-reduced sample; green, a new sample is reduced by dithionite and a spectrum collected 1 min after addition of Fe(III) citrate (100 μM). (*Inset*) Dithionite reduced *minus* oxidized difference spectrum of the MtrCAB MV-proteoliposomes (red) and purified MtrCAB in solution (black) normalized to the maximum signal at 422 nm. (*C*) Baseline-subtracted cyclic voltammograms for adsorbed MtrC, MtrCAB, and MtrA recorded at 30 mV s^{-1}, 0 °C with 3 krpm electrode rotation. Oxidative and reductive peaks (normalized to their respective peak currents) and the normalized integral of the oxidative peak (indicating the extent of protein reduction as a function of potential) are shown as black lines with gray fill and heavy solid lines, respectively. Circles indicate the extent of reduction for each protein as determined by spectrophotometric solution titration. (*D*) Comparison of the redox properties of MtrCAB, MtrC, and MtrA. (*Upper*) Oxidative voltammetric current per mole of protein for MtrC (dashed line) and MtrA (dotted line) and their sum (gray solid line) assuming 10 redox active single-electron hemes per protein. (*Lower*) Oxidative peak currents per mole of MtrCAB (black solid line) compared with the sum of those from the constituents MtrC and MtrA (gray solid line) assuming 20 redox active single-electron hemes in each case. Experimental data as in *C*.

oxidized at ≈0 mV to fully reduced at −450 mV (see circles in Fig. 3*C*). Because spectroscopic changes for a *mono*-heme cytochrome undergoing a single electron transformation typically span ≈200 mV, the potential range spanned by redox transitions of MtrCAB reflects the contribution of multiple hemes with overlapping potentials. Spectropotentiometric titrations of MtrA and MtrC under identical conditions revealed that the hemes of MtrA reduce across a similar potential window to those in MtrCAB, whereas those of MtrC titrate at more positive potentials (Fig. 3*C*). This result suggests that integration of MtrC into the MtrCAB complex results in a negative shift of the operating potential that will increase the driving force for electron transfer from the complexed MtrC to Fe(III) mineral substrates.

The redox properties of MtrCAB and its heme-containing components were explored further by protein film voltammetry (PFV) at basal-plane graphite electrodes. In each case, cyclic voltammetry showed a peak during a reductive scan from 200 to −600 mV, and a peak of similar intensity, but opposite sign, during an oxidative scan from −600 to 200 mV, demonstrating reversible electron exchange with the electrode (Fig. 3*C*). These peaks were not observed in the absence of protein, and they are presented here normalized to their maximum amplitude for ease of comparison (illustrations of raw data before baseline subtraction are provided in Fig. S4). The peaks were unaltered by rapid rotation of the electrodes, or transfer to fresh-buffer electrolyte, which confirms that their origin is adsorbed protein rather than molecules in solution. For scan rates <100 mV s^{-1}, the oxidative and reductive peaks are essentially mirror images with a constant, small peak separation that indicates equilibration between the protein oxidation state and applied potential (Fig. 3*C*). Integration of the current-potential profile reports on the extent of reduction as a function of potential (see the solid curves in Fig. 3*C*) and these superpose well on the data collected from the spectropotentiometric titrations of the proteins in solution (see circles in Fig. 3*C*). Thus, for each protein, the redox activity when absorbed on an electrode is detected across windows of potential comparable with those displayed by the protein in solution. This suggests that all hemes in each protein contribute to the voltammetric response, which is consistent with the high heme-to-peptide ratios of MtrC and MtrA that make it likely the hemes are packed for facile interprotein electron transfer enabling MtrCAB to support electron exchange between MtrC and MtrA in the proteoliposomes.

Taking the voltammetry from MtrC and MtrA to arise from 10 hemes, and that from MtrCAB to arise from 20 hemes, the peak areas averaged for a number of experiments correlate to electrode coverages of 12, 9, and 4 (±1) pmol MtrC, MtrA, or MtrCAB complex cm^{-2}, respectively. If MtrC and MtrA interact with the electrode through a single region of their surface that is not occluded on formation of the MtrCAB complex, the electroactive coverage of MtrCAB could be expected to be similar to that for MtrC or MtrA alone. However, it is likely that many regions of the surface of these heme-rich proteins contact the electrode productively, and that the lower electroactive coverage of the complex reflects there being less exposed surface from either MtrC or MtrA accessible for productive interaction of the MtrCAB complex with the electrode. The voltammetric peaks reveal an uneven distribution of redox activity within each protein. For example, the activity arising from MtrCAB shows that the redox capacity is clustered in two regions with more events at higher, than lower, potentials (Fig. 3*C*). By contrast, MtrA has greater redox activity at lower, rather than higher, potentials, whereas the majority of redox activity from MtrC is contained in a narrower and higher window of potential. The PFV of MtrA and MtrC is similar to that previously published under different conditions (11) in that in both studies the proteins exchange electrons with graphite electrodes over broad potential domains within a window of ≈0 to −400 mV, although there are some differences in the peak shapes and potentials displayed by each protein in the different studies. For the present work, it was important to study MtrCAB, MtrC, and MtrA under identical conditions so that direct comparison of their properties could be made. In this way, it was found that the response of MtrCAB cannot be described simply by adding the response of MtrA to that of MtrC with scaling of the peak areas to reflect contributions from 20, 10, and 10 hemes, respectively (Fig. 3*D*). Thus, the high fidelity of the PFV responses complements the spectropotentiometric results in suggesting that the redox properties of MtrC and MtrA are modulated on formation of the MtrCAB complex. The PFV peak areas for MtrCAB, MtrC, and MtrA were invariant when scan rates were varied between 30 to 30,000 mV s^{-1}, demonstrating that all of the

redox centers maintained communication with the electrode, either directly or via interheme electron transfer, for this scan rate range. Increased peak separation was apparent at higher scan rates, which allowed the standard interfacial electron transfer rate constants to be estimated from "trumpet plots" (11–13) of the data (Fig. S5) as $\approx$195 s^{-1} for MtrCAB, $\approx$220 s^{-1} for MtrC, and $\approx$60 s^{-1} for MtrA. The similar rate constants observed for MtrCAB and MtrC suggests these proteins interact with the electrode in an analogous manner and most likely via their common component, MtrC. The 3- to 4-fold lower rate constant displayed by MtrA suggests that, in the MtrCAB complex, it is MtrC, rather than MtrA, that interacts primarily with the electrode surface, with electrons then equilibrating rapidly between the MtrC and MtrA hemes.

Impact of *mtrA*, *mtrB*, and *mtrC* Deletions on Assembly of the MtrCAB Complex. To investigate the structural organization of the MtrCAB complex, a mutant of *S. oneidensis* lacking the OM *deca*-heme cytochromes MtrC and OmcA was examined to explore whether a stable MtrAB complex could be assembled in the absence of MtrC. Both MtrA and MtrB could be detected in membranes prepared from cells grown anaerobically with Fe(III) citrate as electron acceptor and, after membrane solubilization in TX100, they could be copurified (Fig. 1). Analysis by SDS/PAGE confirmed the absence of MtrC, and the presence of both the $\approx$85-kDa MtrB and $\approx$40-kDa MtrA polypeptides (Fig. 1*B*), the latter of which exhibited heme-dependent peroxidase activity (Fig. 2*A*). The identity of the MtrB protein was confirmed using anti-MtrB antibodies and MALDI-TOF analysis. Notably, MtrB did not stain for heme (Fig. 1*A*). It was not possible to separate MtrA from MtrB in the MtrAB complex under nondenaturing conditions using either gel-exclusion, anion-exchange, cation-exchange, or hydrophobic chromatography in either the oxidized or reduced states. SE was used to determine the stoichiometry of MtrA:MtrB. Profiles were collected from 0.3 and 2.5 μM samples at rotation speeds of 7, 9, and 11 krpm. The data for each concentration could be fitted to a single-species, noninteracting model (Fig. 1*A*) that yielded averaged molecular masses of 112 kDa (0.3 μM) and 110 kDa (2.5 μM), similar to those expected from a 1:1 complex of MtrAB. Plots of ln absorbance versus $(r^2 - r^2_{ref})/2$ approximated to straight lines, consistent with a single homogenous species, but comparison with those of MtrCAB collected in similar conditions revealed a shallower slope for MtrAB, reflecting the lower mass of MtrAB due to the absence of MtrC (Fig. 2*A*). The oxidized UV-vis spectrum of MtrAB displayed a γ- and β-peaks at 410 and 540 nm. On reduction with dithionite, the γ-peak shifted to 422 nm, and α- and β-peaks developed at 552 and 523 nm, respectively. There was no suggestion of a spectral contribution arising from high-spin ferric heme (i.e., shoulders at 600–630 nm). We attempted to obtain PFV of MtrAB using the conditions established for the study of MtrCAB, MtrC, and MtrA. However, we were unable to detect a substantive signal, which could be explained if MtrA associates with MtrB such that a key surface of MtrA required for interaction with the electrode is occluded when MtrA is bound by MtrB. This scenario would be consistent with argument that MtrC, rather than MtrA, that predominantly makes electrical contact with the electrode in PFV of the MtrCAB complex.

The assembly of stable 1:1 complex of MtrAB in the absence of MtrC leads us to suggest that the MtrCAB complex should be considered as two functional components: (*i*) the MtrAB transmembrane electron transfer module; and (*ii*) the MtrC extracellular reductase module. To assess whether it is possible to reconstruct the MtrCAB complex from its component modules, MtrAB and MtrC were mixed together at two equimolar concentrations (0.1 and 0.4 μM), and the mixtures analyzed by SE at three rotation speeds (7, 9, and 11 krpm). For each concentration, the plot of ln absorbance versus $(r^2 - r^2_{ref})/2$ gave an approximate straight line that could be fitted to a single homogenous species of $M_w^{av} \approx$ 210 kDa (Fig. 2*B*). Separate analysis of MtrC confirmed that it existed as a homogenous monomer of $\approx$90 kDa under these conditions. Thus, the M_w^{av} of $\approx$210 kDa for the homogenous species determined for the 0.1 and 0.4 μM mixtures of MtrC and MtrAB accounts for the masses of both MtrAB and MtrC, and suggests a K_d for the MtrC + MtrAB $\leftrightarrow$ MtrCAB equilibrium of $<$0.1 μM.

Having established that a stable integral membrane MtrAB module can assemble in vivo despite the absence of MtrC, we then assessed the fate of MtrA if MtrB was not available as a protein partner. Analysis of MtrA localization in an *mtrB* deletion strain showed that, whereas in the parent strain MtrA localized to the membrane (insoluble) fraction, it localized to the soluble fraction in the absence of MtrB (Fig. 1*C*). This result is consistent with the bioinformatic predictions that MtrA is a water soluble protein, and illustrates the importance of MtrB for the localization of MtrA to the membrane fraction. We next assessed whether an MtrBC complex could assemble in the absence of MtrA by probing for MtrB in whole cell lysates. The MtrB protein can be detected by anti-MtrB antibodies in lysates prepared from WT cells, but is absent from a Δ*mtrB* mutant (Fig. 4*A*, lanes 1 and 2). Significantly, however, MtrB protein could not be detected by anti-MtrB antibodies in lysates from *S. oneidensis* Δ*mtrA* (Fig. 4*A*, lane 3). However, *mtrB* transcripts were detected by PCR, confirming that the gene was transcribed (Fig. 4*B*). Complementation of the Δ*mtrA* strain by *mtrA in trans* restored the production of MtrB to a detectable level (Fig. 4*A*, lane 4), which confirms that the *mtrA* deletion has no polar affect terminating transcription of *mtrB*. These results show that assembly of an OM MtrB, and therefore, an MtrBC complex, is compromised in the absence of MtrA. The functional impact of the absence of MtrA or MtrB for the intact cell was investigated by characterizing the ability to reduce different forms of Fe(III) and Mn(IV) as terminal electron acceptors. Deletion of either *mtrA* or *mtrB* resulted in severe Fe(III) and Mn(IV) reduction deficiencies regardless of the form of these electron acceptors [i.e., ferrihydrite (FH) v soluble Fe(III) citrate], a result consistent with the observations that the *mtrA* deletion mutants fail to assemble MtrB (Fig. 4 *C–E*). Complementation of the Δ*mtrA* and Δ*mtrB* mutant with a WT copy of the *mtrA* and *mtrB*, respectively, restored the WT phenotype (Fig. S6), confirming that the *mtrB* expression plasmid is functionally competent. However, cross-complementation of the Δ*mtrA* strain with the *mtrB* expression plasmid did not restore activity to the mutant (data not shown) and did not lead to MtrB detection in the membrane fraction (Fig. 4*A*, lane 5). These whole-cell experiments confirm that a functional MtrAB module is essential for the electron transfer to the extracellular substrates, and show that MtrA is required for correct assembly of MtrB.

Protein–Protein Interactions in the MtrCAB Complex. The liposome experiments showed that electron exchange can occur between MtrA and MtrC in an MtrCAB complex that can move electrons across a lipid bilayer. However, the distance between the inner and outer faces of the OM ($\approx$40 Å) is too far for unmediated electron transfer between MtrA and MtrC hemes if they lie on these opposite faces of the OM (14). The predicted β-barrel structure of MtrB, and its tight interaction with MtrA, raises the possibility that MtrA may partially embed within the MtrB β-barrel at the inner face of the OM where it could then potentially interact directly with MtrC within MtrB β-barrel. Thus, SE was used to assess whether MtrC and MtrA have the capacity to make a protein–protein interaction. First, to derive the molecular mass of the solution state conformations of MtrC and MtrA in isolation from one another, each protein was subjected separately to SE analysis at multiple rotation speeds (6, 8, and 10 krpm) and a range of protein concentrations (0–20 μM). The M_w^{av} values derived from global nonlinear regression analysis of the combined experimental data were $\approx$90 kDa for MtrC and $\approx$40 kDa for MtrA. These values were in agreement with the predicted molecular mass of each protein,

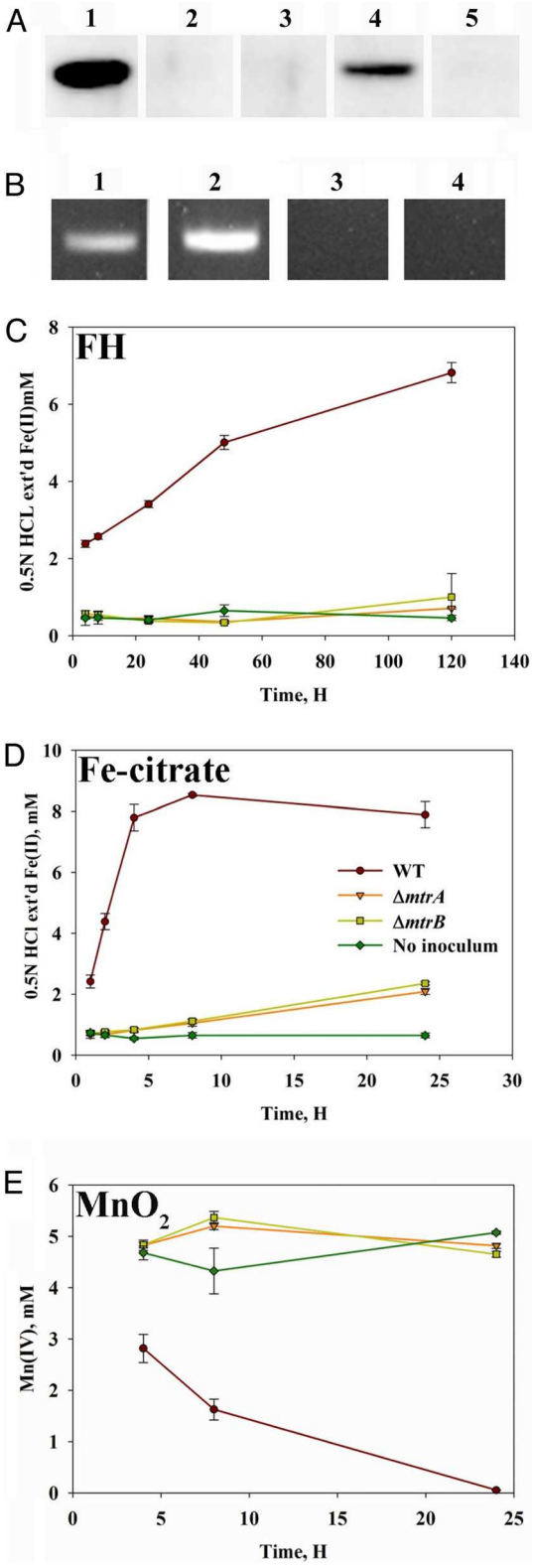

Fig. 4. Characterization of *mtrA* and *mtrB* mutants. (*A*) Immunoblot of cell lysates reacted with antibody specific for MtrB. Lane 1, WT MR-1; lane 2, Δ*mtrB*; lane 3, Δ*mtrA*; lane 4 Δ*mtrA*(*mtrA*$_c$); lane 5, Δ*mtrA*(*mtrB*$_c$). (*B*) Agarose gel electrophoresis of product generated from RT-PCR of WT (lanes 1 and 3) and Δ*mtrA* RNA extracts (lanes 2 and 4). RNA extracts were also treated in the absence of reverse transcriptase enzyme to verify complete digestion of contaminating DNA (lanes 3 and 4). (*C*–*E*) Ferrihydrite (FH), Fe(III)-citrate or Mn(IV)O_2 reduction kinetics of WT, Δ*mtrA*, Δ*mtrB*. Error bars represent SDs from three replicates.

revealing that MtrA and MtrC are monomers in solution over the concentration range studied. The difference in mass between MtrC and MtrA is also reflected in the slope of the lines for each concentration in plots of ln absorbance versus $(r^2 - r^2_{ref})/2$ when compared at the same rotation speed (Fig. 2*C*). Next, 1:1 stoichiometric mixtures of MtrA and MtrC (15, 5, and 0.5 μM) were analyzed. When the data collected at 0.5 μM was fitted to a single component model it gave a M_w^{av} of ≈61 kDa, which does not correspond to the mass measured by SE under similar conditions of either MtrA (40 kDa), MtrC (90 kDa), or the MtrAB complex (110 kDa), suggesting that a single component fit is not appropriate. Notably, the data collected at 15 μM and fitted the same way gave a higher $M_w^{av}$of ≈85 kDa. Because we established that the M_w^{av} of MtrC and MtrA measured by SE is constant over the 0.5–20 μM concentration range when each is analyzed in isolation, then, the observed increase in M_w^{av} of the MtrC + MtrA mixtures most likely reflects a molecular interaction between MtrC and MtrA. Data collected at a range of concentrations and centrifugal velocities (Fig. S7) was, thus, fitted to a two-component hetero-association model and yielded an excellent fit for a K_d for the MtrA + MtrC ↔ MtrAC equilibrium of 11 ± 4 μM. This is much higher than that for the MtrAB-MtrC equilibrium (estimated at <0.1 μM), illustrating the importance of MtrB in stabilizing the MtrCAB complex, but also is consistent with the possibility that MtrA and MtrC make contact in the MtrCAB complex.

MtrAB Modules: A Phylogenetically Widespread Means of Electron Exchange Between a Bacterium and the Extracellular Environment. We have previously noted significant sequence similarity between the *penta*-heme electron transfer protein from *Escherichia coli* NrfB and MtrA (15, 16), and a homology model can be constructed for the first four hemes of MtrA using NrfB as a template (Fig. S8). NrfB houses a ≈50-Å electron wire in a protein that is ≈30 Å in diameter (15). A diameter of this order for the MtrA heme wire would make insertion into the MtrB β-barrel a conceptual possibility, given the expected large pore size of a 28 strand OM porin. For example, the 22 strand β-barrel FepA has a diameter of ≈35 Å with a pore that accommodates a globular N-terminal domain of 150 aa (17). An MtrB pore that enables contact to form between MtrA and MtrC may, thus, allow for the electron exchange between the two proteins suggested by PFV, proteoliposome, and SE experiments. If MtrAB forms a tightly bound OM complex, it raises questions of how electrons reach the complex from the IM. Genetic evidence has strongly implicated an IM quinol dehydrogenase CymA in Fe(III) respiration (2), but it is probable that soluble periplasmic electron carriers mediate electron transfer between CymA and the MtrAB complex. The "MtrAB" electron transfer module may represent a solution to electron exchange across the OM in a range of respiratory systems and bacterial phyla (Fig. 5). The respiratory flexibility of *Shewanella* species includes the ability to use DMSO. In *E. coli*, the active site of the DMSO reductase, a molybdo-enzyme, is located in the periplasmic compartment. However, *Shewanella* are configured to respire extracellular forms of DMSO by localizing the catalytic subunit to the outside of the cell (18). The genes encoding the catalytic subunits, *dmsA* and *dmsB*, cluster with *dmsE* and *dmsF* that encode homologues of MtrA and MtrB (19), suggesting a similar mechanism for moving electrons across the OM. Homologues of MtrA and MtrB (PioA and PioB) are also associated with phototropic Fe(II) oxidation in *Rhodopseudomonas palustris* (19). In this case, electrons could be moving into, rather than out of the cell, from extracellular Fe(II). Our bioinformatic analysis further suggests that *mtrAB* homologues are phylogenetically spread across α, β, and γ proteobacteria and acidobacteria where they can often be found as contiguous genes on the chromosome (Fig. 5; Fig. S1). To our knowledge, their role has not yet been investigated, but functional diversity may be achieved by nonconserved regions that confer specificity for interactions with distinct periplasmic and extracellular proteins.

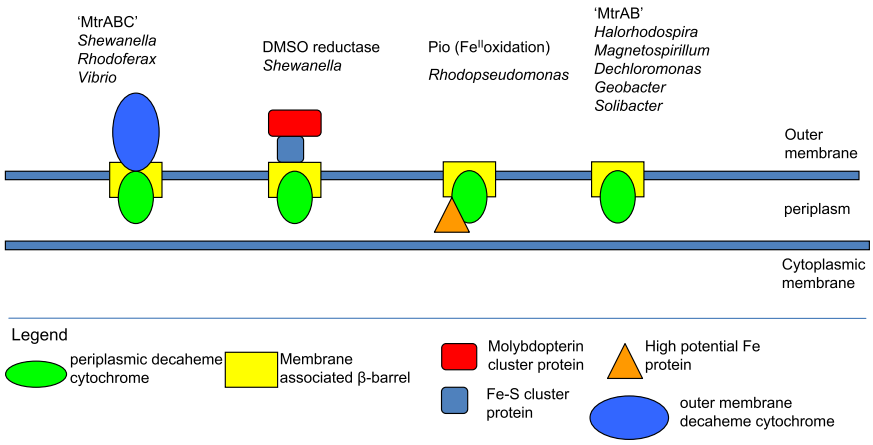

Fig. 5. MtrAB homologues in a range of phyla and OM electron transport systems.

Materials and Methods

Protein Purification and Analysis. Purification of MtrC, MtrA, and MtrCAB was as described previously (5, 6, 12). MtrAB was purified from the Δ*mtrC omcA* strain. Membrane fractions were solubilized in 5% TX100 (20 mM Hepes/100 mM NaCl, pH 7.6) and subjected to Q-Sepharose anion exchange chromatography and Superdex S-200 HR 10/30 gel filtration. SE analysis was performed as described (6, 12). Experiments were carried out in 50 mM Hepes/200 mM NaCl/5% (wt/vol) TX100, pH 7.6. Data were analyzed using Ultrascan and fitted to either a one or two component hetero-association model (20). Spectropotentiometric titrations were performed as indicated (13) in 100 mM Hepes/100 mM NaCl, pH 7.6/5% (wt/vol) TX100 at 15 °C. PFV was performed as described (13), and interfacial electron transfer rates were calculated according to refs. 11–13. Voltammetric data in Fig. 3 is presented as the average of five successive scans for improved signal to noise.

Genetic Manipulation and Expression Analysis. In-frame deletion mutants were constructed according to ref. 21, and were complemented using pBBR1MCS-5 (22). For expression analysis, strains were cultured overnight at 30 °C in Luria–Bertani medium. Proteins blotted onto nitrocellulose membranes were probed with antibodies toward MTRA, MtrC and MtrC (23, 24) and developed using enhanced chemiluminescence. Gene transcription was analyzed in cells cultured overnight in trypticase soy broth (TSB). RNA was extracted using the RNeasy extraction kit (Qiagen) and treated with RQ1 DNase (Promega). RT-PCR was performed using the cMaster RTplusPCR kit (Eppendorf) using primers were designed for a ≈400-bp internal region of *mtrB*. Plasmids, strains, and primers are described in Table S1.

Metal Reduction Kinetics. Overnight cultures were purged with N_2, transferred (final OD_{600} of 0.075) to Balch tubes containing 10 mL of anaerobic M1 medium (2) supplemented with 10 mM silica-stabilized ferrihydrite, Fe(III) citrate or $Mn(IV)O_2$ (30 °C, 25 rpm). Fe(II) was quantified from 0.5N HCl extracted samples. For Mn(IV) measurement, 100 μL of sample was mixed with 1 mL [0.4 mM benzidine-HCl/0.1% glacial acetic acid] in 50 mM Hepes buffer, pH 7.0, and the absorbance measured at 424 nm after a 2-min incubation.

Preparation of Proteoliposomes. Phosphatidylcholine (10 mg mL^{-1}) was added to 1 mL 50 mM Hepes/2 mM $CaCl_2$/10 mM MV. This mixture was sonicated (3 × 40 s) and centrifuged (13,000 rpm × 5 min) to pellet solid material. The supernatant was centrifuged (80,000 rpm × 40 min at 4 °C) and the liposomes pellet resuspended in 1 mL 50 mM Hepes/2 mM $CaCl_2$/MtrCAB (0.2 μM) added. The proteoliposomes were freeze/thawed in liquid nitrogen twice, biobeads (0.25g mL^{-1}) added to remove detergent, and the mixture stirred at 4 °C for 1 h. The Biobeads were removed, and the proteoliposomes centrifuged (80,000 rpm × 40 min) twice. Each time, the pellet was resuspended in 1 mL of 50 mM Hepes/2 mM $CaCl_2$. For experiments, 300 μL of the final proteoliposome suspension were diluted into the same buffer.

ACKNOWLEDGMENTS. We thank the reviewers and editor of the article for helpful comments during the revision process. The EMSL Scientific Grand Challenge was performed in part at the Environmental Molecular Sciences Laboratory (EMSL), a national scientific user facility sponsored by the Department of Energy's Office of Biological and Environmental Research and located at Pacific Northwest National Laboratory (PNNL). PNNL is operated for the Department of Energy by Battelle. J.N. and S.B. were supported by the National Science Foundation (Grant EAR 05-19144). M.T., J.N., and D.R. were supported by the Center for Environmental Kinetics Analysis (NSF CHE-0431328 and the U.S. Department of Energy, Biological and Environmental Research). D.J.R. is a Royal Society Wolfson Foundation Merit Award holder.

1. Richardson DJ (2000) Bacterial respiration: A flexible process for a changing environment. *Microbiology* 146:551–571.
2. Myers CR, Myers JM (2000) Role of the tetraheme cytochrome CymA in anaerobic electron transport in cells of *Shewanella putrefaciens* MR-1 with normal levels of menaquinone. *J Bacteriol* 182:67–75.
3. Myers CR, Myers JM (1997) Outer membrane cytochromes of *Shewanella putrefaciens* MR-1: Spectral analysis, and purification of the 83-KDa c-type cytochrome. *Biochim Biophys Acta Biomem* 1326:307–318.
4. Myers CR, KH Nealson (1988) Bacterial manganese reduction and growth with manganese oxide as the sole electron acceptor. *Science* 240:1319–1321.
5. Pitts KE, et al. (2003) Characterization of the *Shewanella oneidensis* MR-1 decaheme cytochrome MtrA. *J Biol Chem* 278:27758–27765.
6. Ross DE, et al. (2007) Characterization of protein-protein interactions involved in iron reduction by *Shewanella oneidensis* MR-1. *Appl Environ Microbiol* 73:5797–5808.
7. Lower BH, et al. (2009) Antibody-recognition force microscopy shows that outer membrane cytochromes OmcA and MtrC are expressed on the exterior surface of *Shewanella oneidensis* MR-1. *Appl Environ Microbiol* 75:2931–2935.
8. Shi L, et al. (2008) Direct involvement of type II secretion system in extracellular translocation of *Shewanella oneidensis* outer membrane cytochromes MtrC and OmcA. *J Bacteriol* 190:5512–5516.
9. Marsili E, et al. (2008) *Shewanella* secretes flavins that mediate extracellular electron transfer. *Proc Nat Acad Sci* 105:3968–3973.
10. Beliaev AS, Saffarini DA (1998) *Shewanella putrefaciens mtrB* encodes an outer membrane protein required for Fe(III) and Mn(IV) reduction. *J Bacteriol* 180:6292–6297.
11. Firer-Sherwood M, Pulcu GS, Elliott SJ (2008) Electrochemical interrogations of the Mtr cytochromes from *Shewanella*: Opening a potential window. *J Biol Inorg Chem* 13:849–854.
12. Hartshorne RS, et al. (2007) Characterization of *Shewanella oneidensis* MtrC: A cell-surface decaheme cytochrome involved in respiratory electron transport to extracellular electron acceptors. *J Biol Inorg Chem* 12:1083–1094.
13. Hirst J, Armstrong FA (1998) Fast-scan cyclic voltammetry of protein films on pyrolytic graphite edge electrodes: Characteristics of electron exchange. *Anal Chem* 70:5062–5071.
14. Kerisit SN, Rosso KM, Dupuis M, Valiev M (2007) Electronic coupling between heme electron-transfer centers and its decay with distance depends strongly on relative orientation. *J Phys Chem C* 111:11363–11375.
15. Clarke TA, Cole JA, Richardson DJ, Hemmings AM (2007) The crystal structure of the pentahaem c-type cytochrome NrfB and characterisation of its solution-state interaction with the pentahaem nitrite reductase, NrfA. *Biochem J* 406:19–30.
16. Clarke TA, et al. (2008) The role of multihaem cytochromes in the respiration of nitrite in *Escherichia coli* and Fe(III) in *Shewanella oneidensis*. *Biochem Soc Trans* 36:1005–1010.
17. Schulz GE (2002) The structure of bacterial outer membrane proteins. *Biochim Biophys Acta Biomemb* 1565:308–317.
18. Gralnick JA, Vali H, Lies DP, Newman DK (2006) Extracellular respiration of dimethyl sulfoxide by *Shewanella oneidensis*. *Proc Natl Acad Sci USA* 103:4669–4674.
19. Jiao Y, Newman DK (2007) The *pio* operon is essential for phototrophic Fe(II) oxidation in *Rhodopseudomonas palustris* TIE-1. *J Bacteriol* 189:1765–1773.
20. Demeler B (2005) UltraScan. *Modern Analytical Ultracentrifugation: Techniques and Methods*, eds Scott DJ, Harding SE, Rowe AJ (Royal Society of Chemistry, London), pp 210–229.
21. Link AJ, Phillips D, Church GM (1997) Methods for generating precise deletions and insertions in the genome of wild-type *Escherichia coli*: Application to open reading frame characterization. *J Bacteriol* 179:6228–6237.
22. Kovach ME, et al. (1995) Four new derivatives of the broad-host-range cloning vector pBBR1MCS, carrying different antibiotic-resistance cassettes. *Gene* 166:175–176.
23. Beliaev AS, Saffarini DA, McLaughlin JL, Hunnicutt D (2001) MtrC, an outer membrane decahaem c cytochrome required for metal reduction in *Shewanella putrefaciens* MR-1. *Mol Microbiol* 39:722–730.
24. Marshall MJ, et al. (2006) c-Type cytochrome-dependent formation of U(IV) nanoparticles by *Shewanella oneidensis*. *PLoS Biol* 4:e268.